CHIRP MODULATED CO2 LASER RADAR OSCILLATOR

A. Stein

United Aircraft Research Laboratories

Prepared for:

Office of Naval Research
Advanced Research Projects Agency

September 1974

UNCLASSIFIED

SECURITY CLASSIFICATION OF THIS PAGE (When Data Entered)

AD 787606

REPORT DOCUMENTATION PAGE

READ INSTRUCTIONS BEFORE COMPLETING FORM

1. REPORT NUMBER: N/A	2. GOVT ACCESSION NO.
3. RECIPIENT'S CATALOG NUMBER	
4. TITLE (and Subtitle): Chirp Modulated CO_2 Laser Radar Oscillator	5. TYPE OF REPORT & PERIOD COVERED: Final Technical Report, 1 Feb 1974 to 31 Aug 1974
	6. PERFORMING ORG. REPORT NUMBER: N/A
7. AUTHOR(s): A. Stein	8. CONTRACT OR GRANT NUMBER(s): N00014-74-C-0218
9. PERFORMING ORGANIZATION NAME AND ADDRESS: United Aircraft Research Laboratories, 400 Main Street, East Hartford, Connecticut 06108	10. PROGRAM ELEMENT, PROJECT, TASK AREA & WORK UNIT NUMBERS: ARPA Order No. 1806, Amendment No. 13
11. CONTROLLING OFFICE NAME AND ADDRESS: Director, Advanced Research Projects Agency, 1400 Wilson Boulevard, Arlington, Virginia 22209, ATTN: Program Management (HX1241)	12. REPORT DATE: September 1974
	13. NUMBER OF PAGES: 39
14. MONITORING AGENCY NAME & ADDRESS (if different from Controlling Office): Office of Naval Research Branch Office, 495 Summer Street, Boston, Massachusetts 02210	15. SECURITY CLASS. (of this report): Unclassified
	15a. DECLASSIFICATION/DOWNGRADING SCHEDULE

16. DISTRIBUTION STATEMENT (of this Report)

A. Approved for public release; distribution unlimited.

17. DISTRIBUTION STATEMENT (of the abstract entered in Block 20, if different from Report)

See Block 16

18. SUPPLEMENTARY NOTES

N/A

19. KEY WORDS (Continue on reverse side if necessary and identify by block number)

CO_2 laser, waveguide laser, pulsed transmitter, chirp frequency format, laser radar.

20. ABSTRACT (Continue on reverse side if necessary and identify by block number)

The objective of this program was to investigate intracavity electro-optical phase modulation of a CO_2 waveguide laser with the aim of constructing a frequency-chirped master oscillator for application in a 10 micron imaging radar. During this six-month program a special phase sampling technique for frequency locking of the modulated master oscillator to an unmodulated reference laser was investigated. An important experimental result was the measurement of the relative phase between the two lasers by this sampling

DD FORM 1 JAN 73 1473 EDITION OF 1 NOV 65 IS OBSOLETE

UNCLASSIFIED

SECURITY CLASSIFICATION OF THIS PAGE (When Data Entered)

technique. The development of the UARL waveguide lasers was continued resulting in a sealed-off, reliable laboratory device of 0.3 W output power and a lifetime of about 1,000 hrs yielding repetitive linear chirps of 75 MHz width and 2 μsec duration.

CHIRP MODULATED CO_2 LASER RADAR OSCILLATOR

by

A. STEIN

UNITED AIRCRAFT RESEARCH LABORATORIES
EAST HARTFORD, CONNECTICUT 06108
(203) 565–4341

September 1974

FINAL TECHNICAL REPORT

This research was supported by the
Advanced Research Projects Agency of the
Department of Defense and was
monitored by ONR under contract
No. N00014–74–C–0218–$49,702
Scientific Contracting Officer - Dr. M. White
1 February 1974 to 31 August 1974.

ABSTRACT

The objective of this program was to investigate intracavity electro-optical phase modulation of a CO_2 waveguide laser with the aim of constructing a frequency-chirped master oscillator for application in a 10 micron imaging radar. During this six-month program a special phase sampling technique for frequency locking of the modulated master oscillator to an unmodulated reference laser was investigated. An important experimental result was the measurement of the relative phase between the two lasers by this sampling technique. The development of the UARL waveguide lasers was continued resulting in a sealed-off, reliable laboratory device of 0.3 W output power and a lifetime of about 1,000 hrs yielding repetitive linear chirps of 75 MHz width and 2 μsec duration.

TABLE OF CONTENTS

LIST OF ILLUSTRATIONS

1.0 INTRODUCTION AND SUMMARY

Modern optical radar systems for surveillance of extra-atmospheric targets call for high doppler and range resolution. This contract is concerned with the development of an appropriate master oscillator for such a system. The final goal here is to employ intracavity electro-optical phase modulation of a CO_2 waveguide laser to obtain a contiguous train of chirp pulses. During each chirp the frequency is to be swept linearly by 500 MHz in 3 μsec and then returned to its original value.

The desired carrier stability and chirp linearity are 200 Hz and 0.1 percent, respectively. Chirp linearity and carrier stability characterize the quality of the wave format and relate to the fidelity of demodulation. During this six-month reporting period a stable, sealed-off, chirp-modulated CO_2 waveguide laser was developed which yielded linear chirps of 75 MHz width and 2 μsec duration for an output power of 0.3 W on the P-20 line. In observing demodulated signals of successive chirps, we determined the chirp-to-chirp optical phase correlation of the master oscillator.

In considering the application of interest, we note that the frequency stability is to be relative to the receiver local oscillator laser. Frequency locking of two unmodulated lasers is a relatively simple task frequently performed in optical transceivers with extra-cavity optical modulation. However, to lock a chirped signal to a reference poses a difficult problem.

During the reporting period a special sampling technique was developed to facilitate such frequency locking. Initiation of each chirp is precisely controlled by a clock pulse. The optical output is photomixed with the beam of the reference laser such that the photoelectric current yields anrf sweep which is then mixed with the output of a stable rf oscillator whose frequency is within the limits of the rf sweep. The final beat note then represents a sweep through DC. It can be shown that for proper conditions the signal amplitude at the DC point (the point of phase reversal) is a measure of the relative optical phase of the two lasers.

The experiments described here demonstrated that this relative phase value varies little from one chirp to the next as long as the interval between chirps is sufficiently short. For double chirps of 42 μs spacing, the demodulated signals showed little variation in amplitude at phase reversal, while for individual chirps one observes random amplitude values from one oscilloscope frame to the next. In other words, the fluctuation in the optical phase of the master oscillator relative to the reference laser was sufficiently slow such that it could be monitored by observation of the chirp to chirp changes in the amplitude of the demodulated chirp signal at phase reversal.

The observed short-term frequency stability is the result of a rigid mechanical resonator construction employing invar rods as main structural members. Concerning the design of our sealed-off CO_2 waveguide laser, several improvements were made. Operating a 1.5 mm x 12.5 cm capillary system at up to 140 torr filling pressure, we obtained 1.75 W without and 0.3 W with an intracavity modulator.

2.0 BACKGROUND

2.1 General

Advanced optical radar systems for surviellance of extra-atmospheric targets require a wideband master oscillator. The goal of this six-month program phase was to assess the possibility of using intracavity electro-optical modulation of waveguide lasers operating at near-atmospheric pressures for broadband frequency-chirped radar, communication, and general surveillance.

Because of an immediate requirement of the Lincoln Laboratory imaging radar system, the program was aimed specifically at obtaining a continuous train of frequency-chirped pulses (Ref. 1).

In the final system the frequency is to be swept through 500 MHz during each pulse of 3 μs duration and then returned to its original value in less than 1 μs. The output power should exceed 300 mW.

The need for operation near atmospheric gas pressure arises from the requirement for a wide tuning range. Conventional CO_2 systems with a typical gas pressure of 10 to 15 torr exhibit less than 100 MHz bandwidth, governed by doppler and pressure broadening. Extension of the tuning range to 1 GHz has been achieved at UARL with an open-cycle CO_2 waveguide laser operating at 250 torr average gas pressure.

By varying the optical length of the UARL waveguide laser resonator with the help of an intracavity CdTe electro-optic phase modulator, we have obtained fast chirp modulation. As the modulation voltage is ramped from zero to the half-wave value, the optical resonator length is increased by one-half optical wavelength (5 μm), corresponding to a frequency shift of $c/2L$, where c is the velocity of light and L the resonator length. The present UARL chirp-modulated laser can be shortened to an optical length of 30 cm corresponding to a spectral range (and maximum chirp width) of $c/2L$ = 500 MHz. The requirements of the chirped wave format are best discussed by a description of the radar imaging process.

2.2 Radar Imaging

As in certain chirp modulated microwave radar systems, the optical imaging radar achieves range resolution by mixing of the returning chirped pulse with a locally generated, matched chirp pulse. Considering a number of individual target points, the radar return consists of several frequency chirps displaced from each other in time due to a spread in the range of the target points (see Fig. 1).

After optical demodulation the signal is mixed with a matching rf chirp wave to yield a range spectrum where each frequency relates to a range position, its spectral intensity being proportional to the effective reflectivity of the associated range point(s). By presenting this spectrum to a filter bank, the signal is sorted into range bins.

For the application of interest, the target assembly is rigid and rotates about an axis inclined to the line-of-sight; the various target points move in range relative to each other generating a corresponding change in the frequencies of the range spectrum. If one measures not only the frequencies of the range spectrum but the phase at each frequency as well, then relative changes in range signified by a shift in phase from pulse to pulse can be detected long before any target point moves through a range resolvable distance. Since the magnitude of the phase shift is linearly related to the target point's position in cross-range, the latter is determined by measuring the pulse to pulse phase shift of the range spectral frequencies. In fact, the phase shift per pulse repetition period is the doppler frequency, and the doppler spread in a given range bin is a trace of the array of the target points in cross-range at that down range position.

These measurements are characterized by a few simple formulae. First, the frequency difference for a range difference ΔR is:

$$\Delta f = f_B \frac{2\Delta R}{cT} , \tag{1}$$

where T is the pulse length and f_B the chirp width.

The smallest detectable frequency difference is approximately equal to the reciprocal of the observation time T; hence

$$\Delta R_{min} = \frac{c}{2f_B} . \tag{2}$$

FIG. 1

RADAR IMAGING

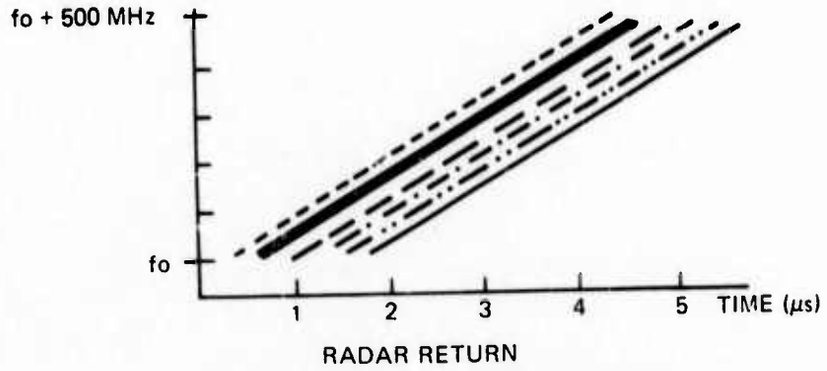

RADAR RETURN

fo = OPTICAL CARRIER FREQUENCY

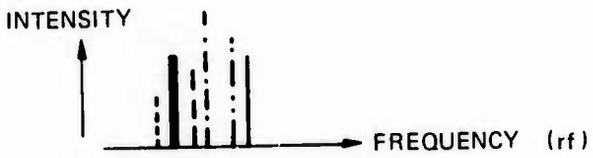

RANGE SPECTRUM

AFTER OPTICAL DEMODULATION AND
MIXING WITH MATCHED rf SWEEP SIGNAL

N09-230-1

It is assumed here that the frequency modulation is sufficiently linear to permit the detection of a 1/T Hz beat note between two time-displaced chirp signals.

The doppler spread of a rotating object is

$$\Delta f_{doppler} = \frac{\Omega L}{c} f_{opt} = \frac{\Omega L}{\lambda} , \tag{3}$$

where Ω is the component of the rotation vector perpendicular to the line-of sight, L is the cross-range extent of the target and f_{opt} is the optical frequency. If the doppler spectrum is observed over N = 1500 contiguous, chirped pulses, the optimum resolution of this measurement is 1/NT, and the resulting cross-range resolution

$$\Delta L = \frac{1}{NT} \frac{\lambda}{\Omega} , \tag{4}$$

(The actual chirp repetition period is somewhat larger than the chirp duration due to a finite fly-back time). Since NT Ω is the projected angle θ through which the target has rotated during the time of the pulse train, one can also write

$$\Delta L = \frac{\lambda}{\theta} . \tag{5}$$

It has been tacidly assumed here that the phase stability of the transmitted wave is sufficient to detect a 1/NT Hz doppler signal.

Furthermore, it is necessary that the frequency ramps are identical throughout the entire pulse train and that initiation of the transmitted and correlation ramps are precisely locked. It is also worth noting that the measurement of the doppler spectrum has an upper limit determined by the pulse repetition frequency, 1/T Hz.

For the Lincoln Laboratory imaging radar the following parameter values have been selected (Ref. 1):

f_B = 500 MHz
T = 3 μs
N = 1500.

The chirp width corresponds to a down range resolution of 30 cm according to Eq. (2).

The cross-range resolution depends on the rotation velocity component Ω; for example, $\Delta L = 30$ can be achieved for a rotational velocity as low as 3 mrad/sec.

The desired specification for the radar waveformat of interest is summarized in Table I.

TABLE I

Chirp Width	f_B = 500 MHz
Pulse Duration	T = 3 μs
Number of Contiguous Pulses	N = 1500
Ramp Linearity	$<1/T$ = 300 kHz
Ramp Initiation Accuracy	1 nsec
Phase Stability	$<1/NT$ = 200 Hz
Wavelength	λ = 10.6μ

2.3 Signal Processing and Timing

The block diagram in Fig. 2 illustrates the essential components of an imaging radar, taken in part from the design of the Lincoln Laboratory system and modified for use of the UARL master oscillator. The chirped waveguide laser is slaved to a stable laser in the manner described in Section 2.6. The local oscillator, which is tunable to permit compensation of the large uniform doppler shift due to the very high translational velocity of the target, is also slaved to the same stable laser; a pre-determined frequency difference is maintained with the help of a VCO, controlled by the system computer in accordance with the target motion. The correlation-detected signal is measured by digitizing its in-phase and quadrature components via 30 MHz, 8 bit A/D converters. A three-dimensional image of the target is then constructed by Fourier analysis of the digitized range and doppler spectrum. The speed of the A/D converters limits the target information bandwidths to 30 MHz, a small fraction of the available 500 MHz band. As a consequence, the unambiguous range spread is limited to 30 m.

FIG. 2

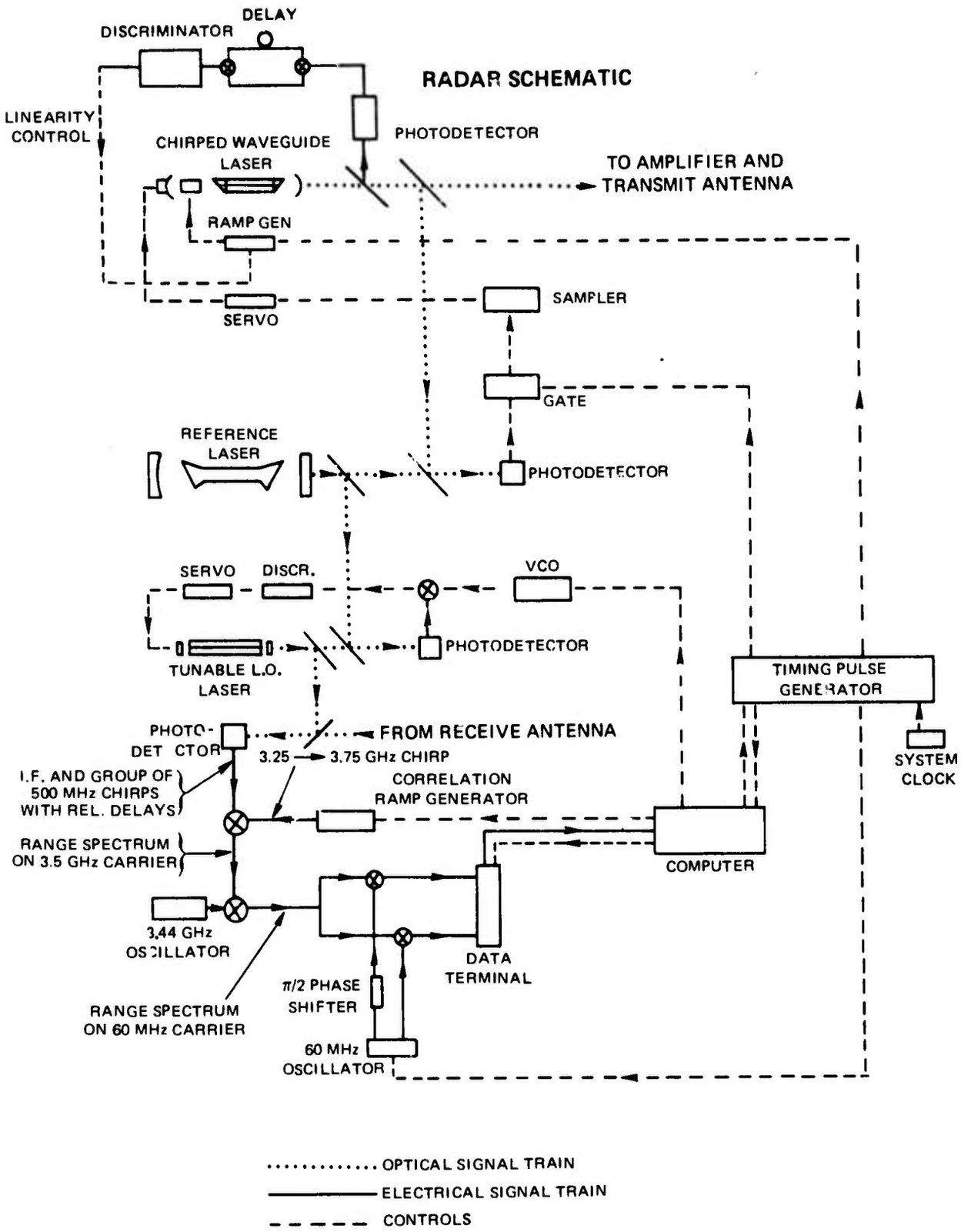

N03-188-4

A possible timing and sequencing system for the transmitted signal of the imaging radar is illustrated in Fig. 3. The basic timing signal is received from a clock and consists of a precise 5 MHz sinusoid. The timing circuits up-converts the 5 MHz signal to 30 MHz and generates a sequence of pulses at this frequency which will be the basic timing pulse sequences for the master oscillator and also controls the A/D conversion circuit. One of these pulses triggers the first ramp; the next ramp then will commence on the 101st timing pulse, the following on the 201st pulse, and so on.

2.4 The Nature of Waveform Distortions

Waveform distortions can be divided into those which perturb the carrier stability and those which affect the modulation quality; i.e., linearity, repeatability and timing of the frequency ramps.

Carrier fluctuations are caused by mechanical and thermal variations of the optical resonator length and variations in the index of refraction of the plasma due to fluctuations of the discharge current. It has been shown that for the short observation periods (5 msec) considered here, mechanical and thermal motion of the resonator structure and the fluctuation in the plasma current can be sufficiently suppressed to obtain the required frequency stability (Ref. 2). The insertion of the modulator crystal into the resonator, however, and the subsequent ohmic heating by the drive signal has to be considered. Let us assume that the modulation is applied continuously and that thermal equilibrium has been established in the sense that the average crystal temperature variation is small and slow. There remains an instantaneous temperature variation synchronized with the ramp voltage, since the characteristic cooling time of the modulator crystal is much larger than the ramp period. It is shown in Appendix I that the resultant thermal frequency sweep varies with the third power in time and for the system proposed here, attains a value of 900 Hz at the end of the ramp period. Although this frequency excursion exceeds the specified tolerance, it is a well-determined carrier shift and may be compensated mathematically in the signal processing procedure.

Any variation of the voltage ramp from the ideal function is directly translated into a proportional deviation of the frequency ramp from its ideal linear profile. This puts the burden of design on the voltage generator which must be fabricated to exceptional specifications of timing and repeatability The required linearization is to be attained by an active feedback loop. Aside from the waveform errors caused by the modulation signal, one must consider the phenomenon of "frequency pulling", an effect inherent in the tuning characteristics of lasers. It has been shown that the so called linear frequency pulling effect of a homogeneously broadened line is described by the formula (Ref. 3)

TIMING SCHEMATIC

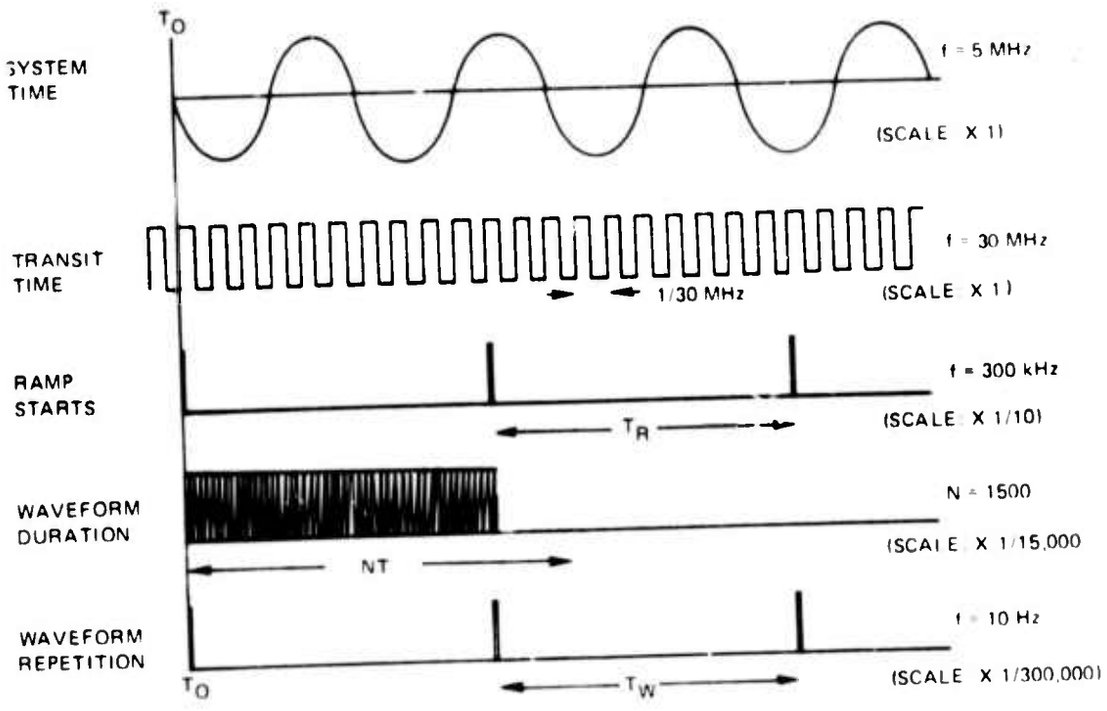

$$\omega - \omega_c = \frac{\Delta\omega_c}{\Delta\omega_a} (\omega_a - \omega_c), \tag{6}$$

where ω is the oscillating circular frequency, ω_c the "cold-cavity" resonance, ω_a the line center of the laser transition, and where $\Delta\omega_c$ and $\Delta\omega_a$ are the half-widths of the passive optical resonance and the molecular transition, respectively. The value $\beta = \Delta\omega_c/\Delta\omega_a$ the so called "stabilization factor," is approximately 1/50 for the system discussed here resulting in a frequency shift of 5 MHz if the laser is detuned by 250 MHz from line center. It should be noted that Eq. (6) is an approximation which holds only in the vicinity of line center. As ω_c approaches the values $\omega_a \pm \frac{1}{2}\Delta\omega_a$, the dispersion becomes distinctly nonlinear.

Equation (6) can be written in the form

$$\omega - \omega_a = (\omega_c - \omega_a)(1 - \beta). \tag{7}$$

Substituting $\omega_c - \omega_a = \alpha t$ for electro-optic tuning, we get

$$\omega - \omega_a = \alpha(1 - \beta)t, \tag{8}$$

where t is the time coordinate, whose zero point is assumed at the instant at which ω_c equals ω_a. According to Eq. (8), the effect of linear mode pulling is to reduce the chirp range by approximately 2 percent ($\beta = 0.02$ for the case of interest) without affecting chirp linearity. Since the tuning range in the case of interest exceeds the range of linear frequency pulling, Eq. (8) represents only an approximation.

2.5 Chirp Linearization

As discussed in Section 2.2, chirp linearity relates to the accuracy with which the range spectrum can be measured. For a chirp duration of T = 3 μs, the maximum resolution is approximately 300 kHz. One would like to keep the frequency error due to ramp non-linearity below that value; i.e., the voltage ramp linearity must be better than 0.06 percent.

While this accuracy may in principle be designed into the voltage generator, a more feasible technique is an active chirp linearization which has been used in microwave radar.

Referring to Fig. 4, it is apparent that the principle of active chirp linearization is quite simple. First, the frequency chirp is transposed from the optical carrier into the rf regime by heterodyning with a stable reference laser. Next, the rf chirp is correlated with itself, i.e., the photoelectric signal is divided into two parts; then one is delayed relative to the other by propagation through a length of coaxial cable and mixed with the former to yield a constant frequency beat-note. FM nonlinearity results in a variation of the beat frequency which is detected in a discriminator whose output voltage and polarity is proportional to the amount and sense, respectively, of the deviation from the nominal beat frequency. This error signal then is used to direct a servo which operates on the grid control of the ramp generator's current regulating pentode (Fig. 5).

Chirp distortion results predominantly from the operating characteristics of the HV regulating pentode. Figure 5 shows a photograph of the ramp generator and its schematic diagram. A possible control circuit is shown in which signal I_x compensates for the fall-off in the pentode characteristic and signal I_y relates to the above described linearization loop.

By observing the error voltage at the discriminator output (Fig. 4), one obtains an instantaneous measure of chirp distortions. A more instructive test of chirp linearity and simultaneously a direct demonstration of range imaging is obtained in an actual range discrimination experiment. One may place two retro-reflectors at different ranges and mix their returns in a photodetector; here the correlation delay is optical rather than electrical. The difference between the actual and the ideal range resolution characterizes the quality of the chirp signal comprehensively.

2.6 Phase Sampling

In discussing the carrier stability of a chirped CO_2 laser, one must distinguish between the electro-optic changes in the oscillation frequency and spurious variations in the optical resonator length caused by thermal and mechanical effects. Of particular interest is the thermal variation in the index of refraction of the modulator crystal, since all other instabilities can be controlled to the required tolerances by passive means; i.e, by an appropriate construction of the laser (Ref. 2).

The term phase has no unequivocal meaning for a chirped signal. In the following we therefore introduce a definition of the phase of a chirped signal which is meaningful for the investigation considered here (see Fig. 6).

FIG. 4

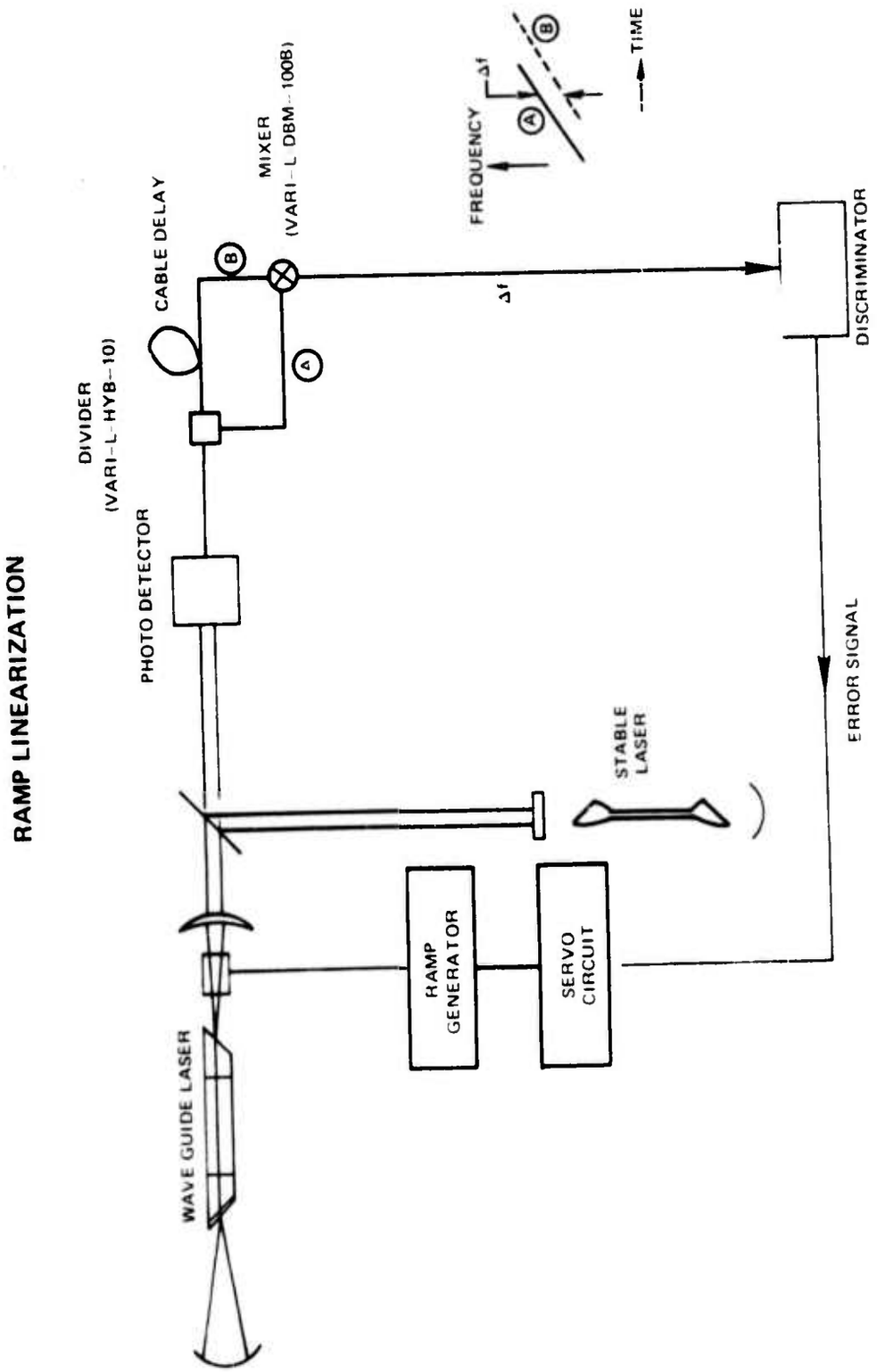
RAMP LINEARIZATION
DIVIDER
(VARI-L HYB-10)
CABLE DELAY
MIXER
(VARI-L DBM-100B)
FREQUENCY
Δf
TIME
DISCRIMINATOR
PHOTO DETECTOR
STABLE
LASER
ERROR SIGNAL
RAMP
GENERATOR
SERVO
CIRCUIT
WAVE GUIDE LASER

FIG. 5

RAMP GENERATOR

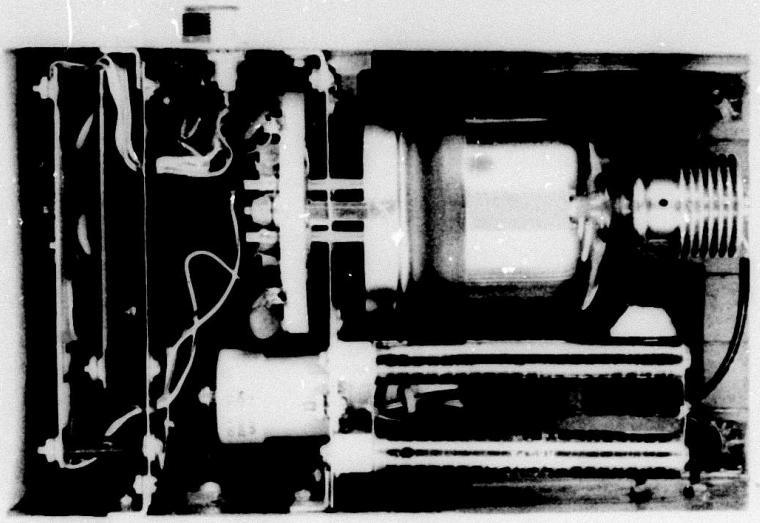

a) RAMP HEAD

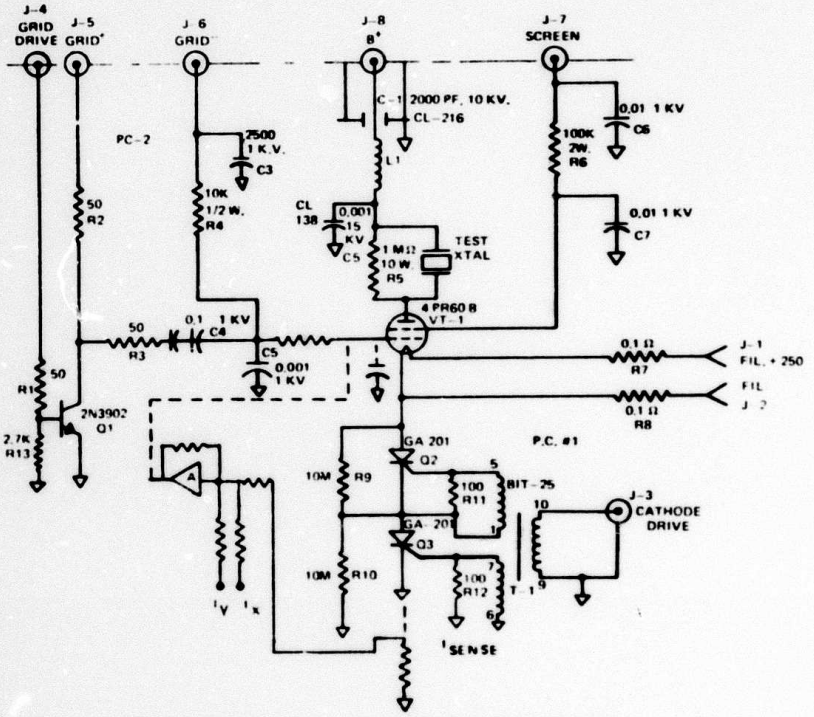

b) HIGH-VOLTAGE RAMP GENERATOR

(DASHED CONNECTION REPRESENT POSSIBLE ADDITIONS FOR FEEDBACK LOOP)

N03-184-1

FIG. 6

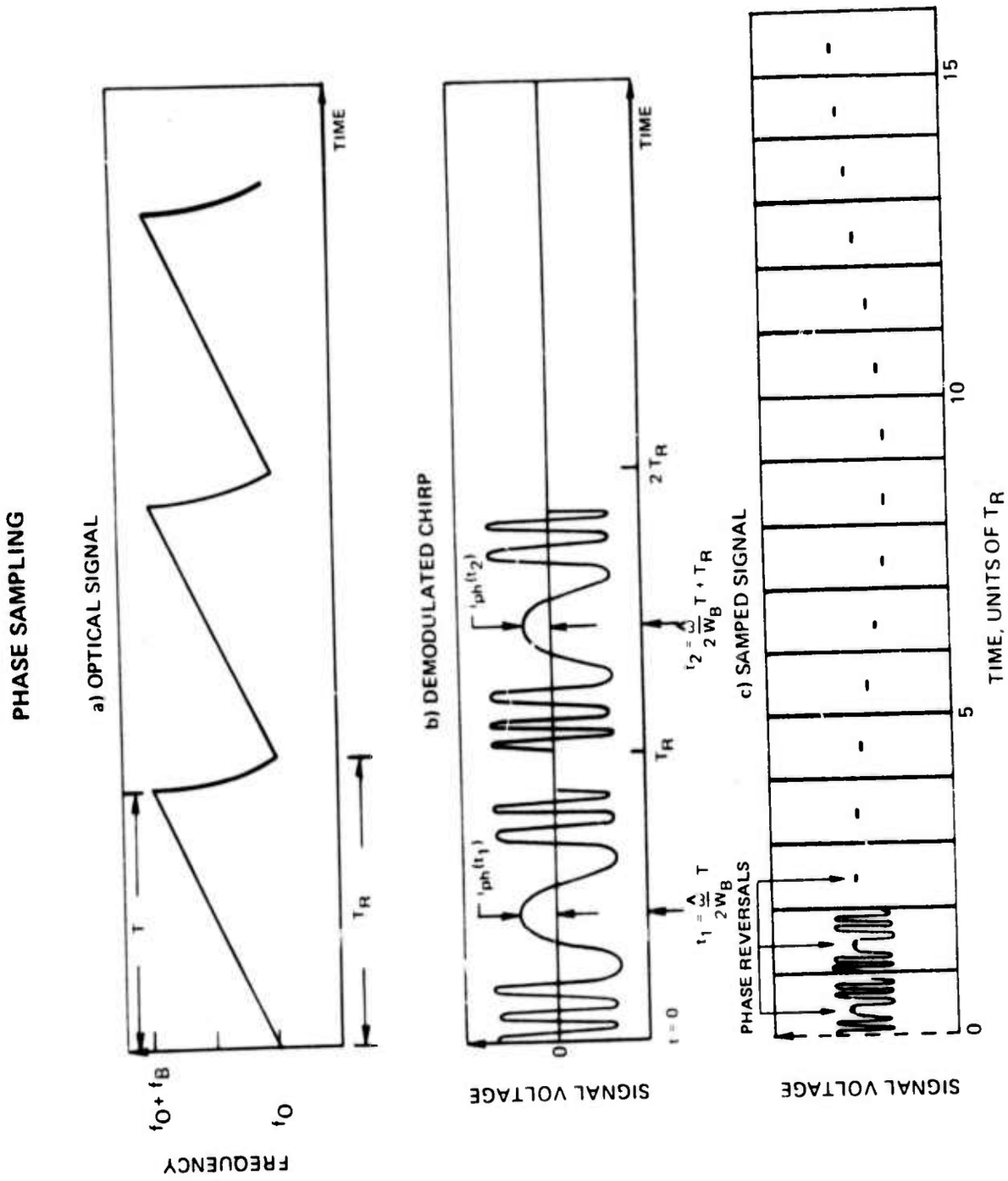

N03-188-2

The photocurrent resulting from mixing the chirped optical signal with a stable reference laser, is given by

$$i_{ph} = \frac{\eta q}{h f} \sqrt{P_s P_{LO}}, \tag{9}$$

where η is the quantum efficienty of the photodetector; q the elementary electric charge and hf the optical quantum energy. P_{LO} and P_s are the instantaneous powers of the reference and signal beam, respectively, given by

$$P_{LO} = 2 \bar{P}_{LO} \sin^2 \left\{ \omega_o t + \frac{\omega B}{T} \cdot t^2 + \varphi(t) \right\} \tag{10}$$

and

$$P_s = 2 \bar{P}_s \sin^2 \{ \omega'_o t \}, \tag{11}$$

where ω_o is the circular frequency of the signal at the beginning of the chirp, ω_B the chirp bandwidth, T the chirp duration, t the time coordinate, ω'_o the circular frequency of the reference beam, $\bar{P}_{LO}$ and $\bar{P}_s$ the time averaged power values of the reference and signal beams respectively; and φ (t) the phase term of interest which represents thermal, mechanical and parasitic electro-optical frequency drifts. The ac photocurrent is then given by

$$i_{ph} = i^o_{ph} \cdot \cos \left[\frac{\omega B}{T} \cdot t^2 - \hat{\omega} \cdot t + \varphi(t) \right]. \tag{12}$$

where $\hat{\omega} = \omega'_o - \omega_o$.

The first two terms in brackets can be expressed by the formula

$$\frac{\omega_B}{T} \left(t - \frac{\hat{\omega}}{2\omega_B} \cdot T \right)^2 - \frac{(\hat{\omega})^2}{4} \cdot \frac{T}{\omega_B}. \tag{13}$$

which yields a minimum value at $t = \frac{\hat{\omega}}{2\omega_B} \cdot T$, subsequently called, the point of phase reversal.

For $t = \frac{\hat{\omega}}{2\omega_B} \cdot T$, we obtain from Eq. (12)

$$\varphi_1 = \frac{(\hat{\omega})^2}{4\omega_B} \cdot T + \text{ARCCOS}\ (i^1_{ph}/i^o_{ph}) , \tag{14}$$

where φ_1 is the phase value, and i^1_{ph} the instantaneous photocurrent at $t = \frac{\hat{\omega}}{2\omega_B} \cdot T$.

In considering Eq. (14), it should be noted that the quantity of interest is the change of φ_1 from chirp to chirp. To render the phase term $\frac{(\hat{\omega})^2}{4\omega_B} \cdot T$ a constant $\hat{\omega}$, T and ω_B must be sufficiently controlled.

If it is assumed that the variation in $\hat{\omega}$ can be neglected, one is only concerned with the variation in the chirp slope, ω_B/T. For $\hat{\omega}$ = 10 MHz and 1 percent chirp slope stability, the average chirp-to-chirp phase error due to the above term is 0.01 radian.

Let us consider a small time period about the point of phase reversal, $t = \delta t + \frac{\hat{\omega}}{2\omega_B} \cdot T$. From Eqs. (12) and (13), we get

$$(i^o_{ph} + \delta i_{ph}) = i^o_{ph} \cdot \cos \left\{ (\delta t)^2 \cdot \frac{\omega_B}{T} - \frac{(\hat{\omega})^2}{4\omega_B} \cdot T + \varphi_1 \right\}, \tag{15}$$

where it is assumed that ω (t) is of essentially constant value during the time period of interest. Eq. (15) indicates that the photocurrent changes very little as long as $(\delta t)^2 \cdot \frac{\omega_B}{T} \ll 2\pi$ or

$$\delta t << \sqrt{\frac{T}{f_B}} \approx 100 \text{ nsec} \tag{16}$$

for our example.

This is an encouraging result in that the dwell time near the constant phase value is much larger than the jitter in the ramp trigger timed by the system's master clock circuit to an accuracy of 1 ns.

The method of sampling and controlling the optical phase of a repetitively chirped signal as illustrated in Fig. 2 is a straightforward technique and has been successfully employed in microwave systems. High-frequency phase fluctuations which exceed the sampling rate (300 kHz) must be suppressed by a rigid mechanical resonator construction and selection of proper discharge conditions.

Slow variation in phase are corrected by a familiar technique in which the sampled signal is used to generate an error signal for corrective piezoelectric resonator tuning. Again, the error signal provides all necessary information on the phase stability but a more comprehensive test is the observation of actual doppler signatures from a laboratory target, for instance a small retro-reflecting mirror mounted on a rotating platform.

3.0 TECHNICAL ACCOMPLISHMENTS

Shortly after the demonstration of the waveguide laser (Ref. 4), UARL embarked on an extensive research program concerning the investigation of these new devices; specifically their use in high-resolution optical radar systems. This program augments a broader UARL effort in the field of 10 micron radar comprising a number of applications such as Laser Obstacle and Terrain Avoidance Warning Systems for Helicopters (LOTAWS) and Optical Discrimination Radar for surveillance of extra-atmospheric targets.

In the course of this program, technical progress has been made on a number of different problems relating to the design of frequency-chirped, stable CO_2 waveguide lasers. These include fabrication of waveguide/plasma tubes of sealed-off and open-cycle design; choice and mounting of resonator optics; line selection; and construction of electro-optic modulators. Much effort at UARL has gone into the fabrication of stable, long lived, efficient and rugged CO_2 waveguide lasers. A tube processing station was assembled and a number of different waveguide/plasma tubes were fabricated and tested. Figure 7 shows a photograph of the laser head used for the experiments discussed below. This unit was operated either open cycle or sealed off. Figure 8 shows the complete experimental setup. A graph of the waveguide laser output versus average gas pressure (open cycle) at 20°C tube temperature and without the modulator is shown in Fig. 9. This performance equals the best previously reported resulted for an equivalent device (Ref. 5). Maximum output power occurs at 190 torr, a result which agrees with recently published data obtained with a 1 mm square channel waveguide laser (Ref. 6). Figure 10 shows heterodyne signals obtained with the setup shown in Fig. 7 where the waveguide laser was operated in a sealed-off fashion. Finally, Fig. 11 shows a compact waveguide system.

3.1 Laser Performance

The steady-stage behavior of a low gain homogeneously broadened CO_2 laser is described by the relation

$$2g\hat{\ell}\,(1 + 2\,P_i/2P_s)^{-1} = \alpha + T, \tag{17}$$

FIG. 7

WAVEGUIDE LASER HEAD

RL74-271-A

FIG. 8

HETERODYNE SYSTEM APPARATUS

RL-74-83-A

NO3 256 1

FIG. 9

LASER POWER VS PRESSURE

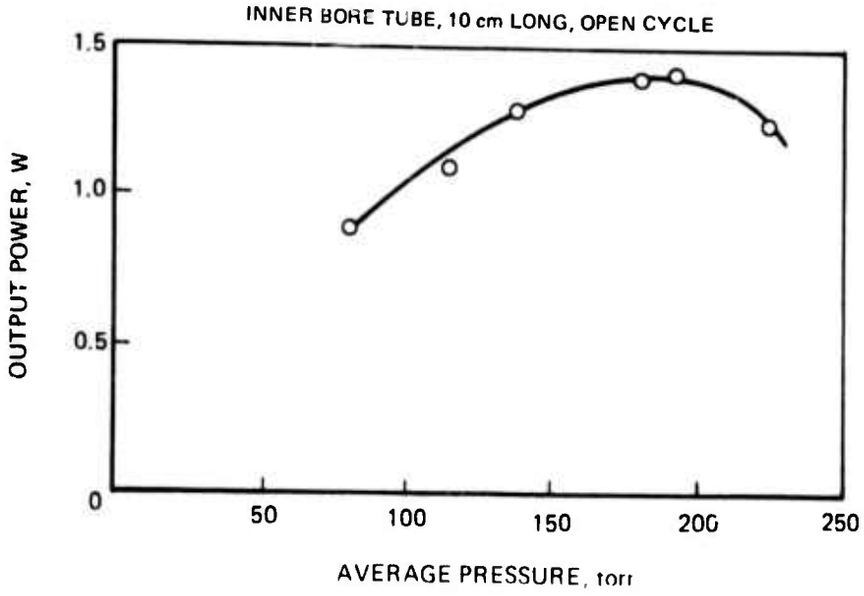

N03-188-3

HETERODYNE SIGNALS

(SPECTRUM ANALYZER DISPLAY)

HORIZONTAL: 10 MHz /div
VERTICAL: LOG SCALE
SCAN SPEED: 3ms/ div
I.F. BANDWIDTH: 10kHz

LINES REPRESENT SAMPLING COINCIDENCES OF SPECTRUM ANALYZER AND SIGNAL

a) QUIET ENVIRONMENT

20 MHz

b) NOISY ENVIRONMENT

20 MHz

N03-229-1

FIG. 11

COMPACT WAVE GUIDE LASER

RL-74-259-A

N09-140-2

where $\hat{\ell}$ is the length of the plasma column, g the unsaturated exponential power gain coefficient per unit length of the active medium, P_i the unidirectional optical power flow inside the resonator, P_s is the saturation power, α is the intracavity loss encountered upon a round-trip through the resonator and T is the relative transmission of the output mirror. Equation (17) states that the power-saturated gain of the active medium has to balance the total optical loss consisting of output coupling and resonator losses (imperfect reflection at the mirrors, imperfect transition from free space to guided propagation, radiation leakage into the capillary wall, absorption in the modulator, and reflection off the modulator faces). The output power is given by $P_o = T \times P_i$, hence

$$P_o = T \cdot \tfrac{1}{2} P_s \left[2g\ell / (\alpha + T) - 1\right]. \qquad (18)$$

Two different UARL waveguide lasers shall be considered as examples; one of open-cycle construction and the other one sealed off.

The open-cycle system employs a BeO tube, approximately 10 cm long, with a 1.0 mm bore. CO_2, N_2 and He are individually metered before they enter a mixing plenum at the ratio (1:1:3) and flow through the plasma vessel into a mechanical vacuum pump. The main pressure drops occur at the entrance and exit of the capillary while the pressure inside the capillary is nearly constant assuming a value midway between the pressure values measured at the gas intake and exhaust ports (Ref. 10). As the flow is increased from 10 to 55 std cm^3/sec, the concomitant capillary pressure rises from 40 to 225 torr. At a flow of 10 std cm^3/sec and an average pressure of 40 torr, the active gas in the 0.08 cm^3 capillary volume is replaced at a rate of 250 times per second. When the open-cycle laser is operated with two concave mirrors whose radii of curvature are 25 and 20 cm and which are coated for high reflectivity and 7.5 percent transmission at 10.6μ respectively, a maximum output power of 1.5 W is measured at 190 torr gas pressure and 20°C tube temperature. If the estimated values $2g\ell = 0.50$, $\alpha = 0.08$ (guiding and mirror losses per round trip) and $T = 0.075$ (measured) are inserted into Eq. (18), a value of 18 W is calculated for the integrated saturation power, P_s. The saturation intensity then is $I_s = P_s/\pi\sigma^2$, where σ is the e^{-1} intensity radius of the Gaussian beam which best matches the EH_{11} waveguide mode. It was shown that $\sigma/a = 0.455$ where a is the capillary radius (Ref. 4). For $a = \frac{1}{2}$ mm, we calculated $I_s = 11.2$ kW/cm^2.

When the modulator crystal was inserted into the open-cycle CO_2 waveguide system, a 50 percent drop in output power was observed. From Eq. (18) and the above parameter values follows that the additional resonator loss introduced by the modulator device is 8 percent. Careful measurements of the CdTe crystal's bulk absorption yielded a coefficient of 0.25 percent/cm; i.e., a 2 percent round-trip absorption loss. To this we add 1 percent loss at each optical interface; 4 percent for one round trip. The difference of 8 percent relates to depolarization loss due to the influence of stresses in the crystal.

The sealed-off waveguide laser used a BeO tube of 1.5 mm ID and 5 in. length. This system was filled with a gas mixture of He, N_2, CO_2, Xe and H_2 in the ratio 4:1:1:0.13:0.1 to a total pressure of 100 torr yielding a maximum power of 1.75 W at 20 deg tube temperature.

Insertion of the modulator crystal led to a reduction in output power to 0.3 W which reflects the fact that the gain in sealed-off systems is lower than for fast flowing open-cycle ones. The modulator insertion loss in this case has a strong effect on the optical output as indicated by Eq. (18). It is thus important to minimize all optical insertion losses. The coating on the two commercially supplied resonator mirrors have average losses of 1 percent. To this we must add the 8 percent round-trip loss introduced by the modulator.

Another source of poor laser performance is an excessive waveguide loss. These losses have been studied in great detail by Abrams and coworkers (Refs. 6 and 9). Our experimental data corroborate their findings; namely, that for well-fabricated BeO waveguides of 1 mm diameter, the coupling losses between guided and free space modes plus the losses due to mechanical imperfection of the waveguide and absorptive or refractive wall losses, can be reduced to below 1 percent per round trip.

For the sealed UARL system the waveguide round-trip loss was estimated at 2 percent. If the value of 2 percent for the output transmission is added to the value of 12 for the resonator insertion loss, we get a value of 14 percent for the threshold gain. At an estimated gain of 3/4 percent/cm and a round-trip capillary length of 25 cm, the round-trip optical gain is about 18 percent which is relatively close to threshold, hence the relatively low output power.

3.2 Chirp Modulation

The intracavity phase modulator consists of a CdTe crystal of 3 x 4 x 40 mm dimension cut for <111> orientation of the 4 x 40 mm faces which are Ag plated to provide electrodes for a drive voltage along the <111> crystal direction, while the beam propagates along the long crystal dimension, parallel to the <110> crystal axis. The indicatrix axes are then parallel and normal to the <111> direction, with maximum electro-optic index variation for an optical polarization parallel to the applied field, characterized by the half wave voltage (Ref. 7).

$$V_{\lambda/2} = \frac{\sqrt{3}\,\lambda \cdot d}{2n_o^3 r_{41} \ell}, \tag{19}$$

where λ is the optical wavelength; d and ℓ are the height and length of the CdTe crystal, respectively; n_o is the intrinsic refraction index of CdTe at the wavelength λ and r_{41} is the relevant electro-optical constant. Inserting $\lambda = 1.06\ 10^{-3}$cm, d = 0.3 cm, ℓ = 4.0 cm and $n_o^3\, r_{41} = 10^{-8}$ cm/V into Eq. (19) yields $V_{\lambda/2}$ = 6.9 kV.

The frequency shift for the applied modulator voltage V is

$$f_B = \frac{c}{\alpha L} \frac{V}{V_{\lambda/2}} \tag{20}$$

where c is the velocity of light and ℓ the optical resonator length. It is apparent that the maximum useful frequency shift occurs for $V = V_{\lambda/2}$ (assuming of course that the half-wave voltage does not exceed the breakdown value of the crystal) and is limited by the attainable values of L. The breakdown field varies somewhat from sample to sample but should exeed 15 kV/cm. (Ref. 8).

In the course of our experiments we observed several voltage breakdowns at much lower fields, but the arc path was either along the sidewall due to insufficient surface cleanliness, or along the coated optical surfaces. Surface arc formation can be eliminated by proper protection of the sidewalls and a slight recession of the electrodes from the edges of the optical faces.

In summary then, a crystal of 4 cm physical (10.7 cm optical) length appears adequate to yield 500 MHz chirp modulation. Adopting the most compact design to yield an optical resonator length of L = 20 cm leaves an adequate length of 10 cm for the plasma tube. The free spectral range of the laser shown in Fig. 7 was 300 MHz. Applying a ramp voltage of 0 → 1750 V to the crystal, we obtained a repetitively chirped output of 75 MHz modulation width. For the phase measurement described below, the ramp voltage had to be precisely repetitive; it was found that our system yielded such performance only for relatively low voltages (< 500 V) which corresponded to a chirp width of 20 MHz.

3.3 Phase Measurements

As discussed in the previous section, the essential step in establishing a carrier stabilization loop is the sampling of the demodulated signal's amplitude at phase reversal. By following that sampled value from chirp to chirp, we can determine the phase drift between the master oscillator and the reference laser. It is important that the phase drift between chirps is small, or expressed differently, that the sampling rate exceeds the rate of phase change. To determine the feasibility of this approach, we conducted an experiment whose setup is illustrated in Fig. 12. The master oscillator is chirped over 20 MHz and its output was optically mixed with the reference laser such that the IF frequency sweeps from 10 to 30 MHz. This photoelectric sweep signal was then mixed with a 20 MHz rf-signal to yield a sweeping beat note, -10 to +10 MHz, going through DC, which is displayed in the oscillograms of Fig. 13 together with the voltage ramp applied to the intra-cavity CdTe modulator crystal.

We could, of course, also have used the photomixing step itself to obtain such a sweep signal going through DC. In that case one needs, however, an rf-amplifier whose spectral range extends to DC. Since the amplifiers available to us had a spectral range of 2 to 500 MHz, we resorted to the above described method where the photoelectric output swept between 10 and 30 MHz and after amplification was mixed with an rf sinusoid.

In considering the oscillographs shown in Fig. 13, we notice two DC points: one associated with the down ramp, the other with the fly-back of the modulator drive, both occuring at the same voltage value as expected. Note also that the position of the phase reversal points and their amplitude values vary randomly from frame to frame. In this experiment, each chirp was triggered by a gate pulse from the oscilloscope in "single sweep" operation such that the relative optical phase between master and reference lasers is arbitrary. While it is not necessary to obtain a particular signal value at phase reversal, we are interested in the change of this value from one chirp

FIG. 12

PHASE MEASUREMENT FOR CHIRPED LASER

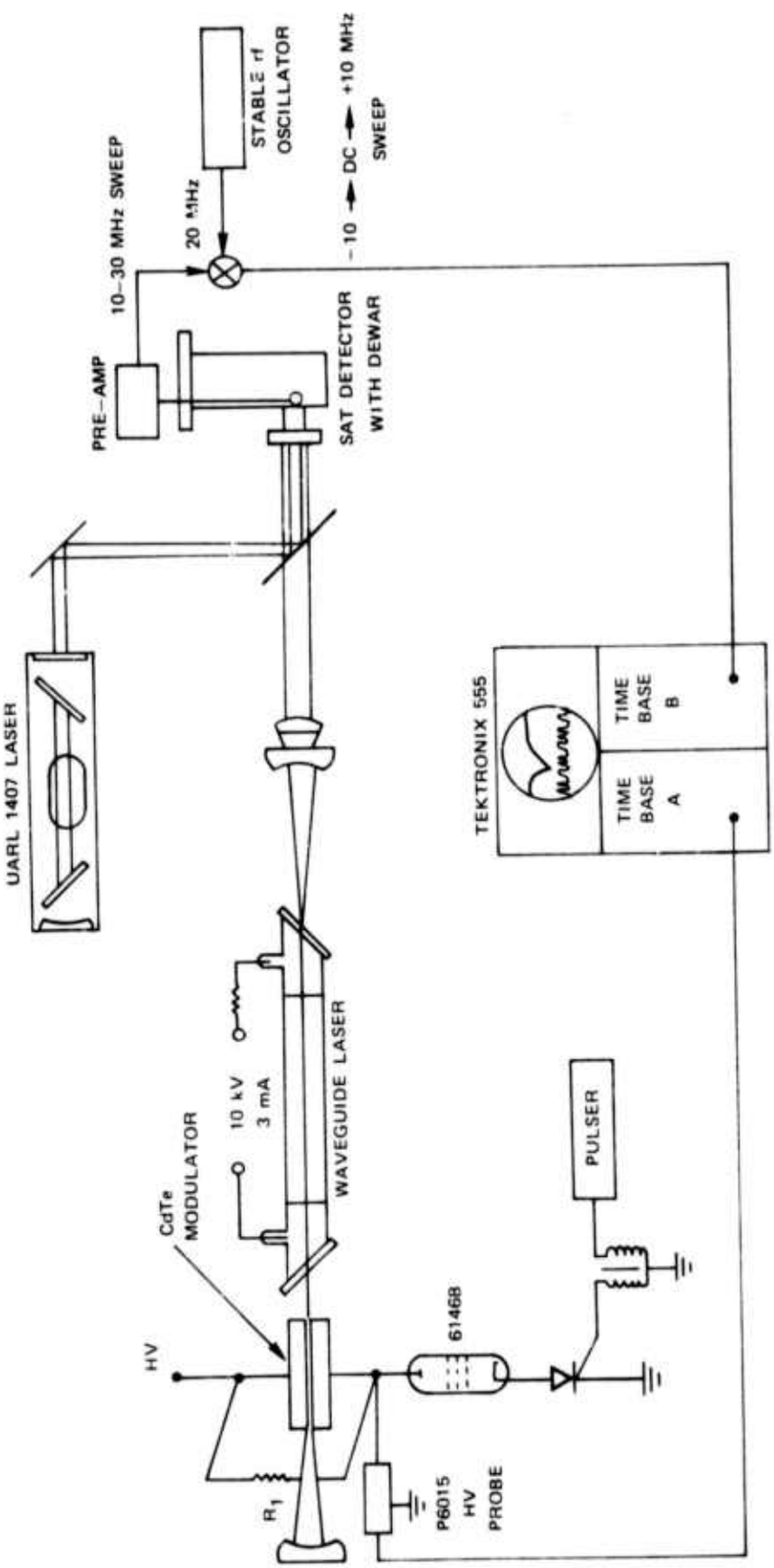

N09-94-1

FIG. 13

SINGLE CHIRPS

MODULATOR VOLTAGE

DEMODULATED SIGNAL

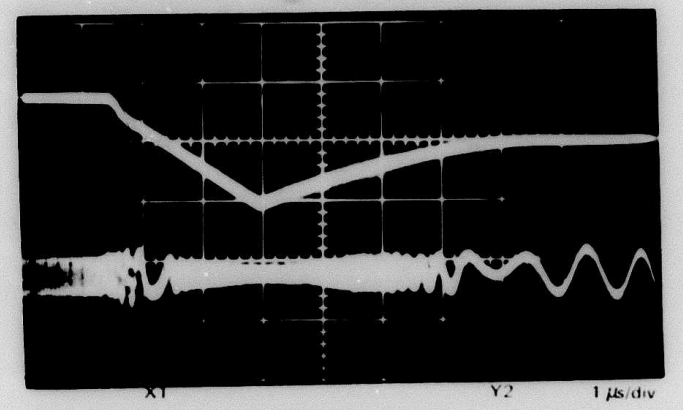

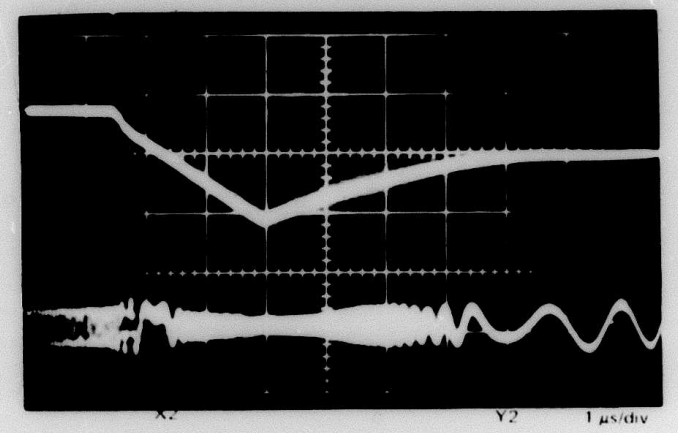

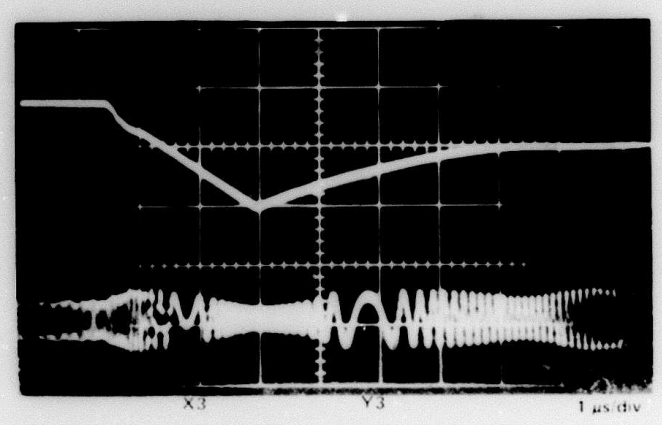

N09-122-2

to the next. To investigate that phenomenon, we performed a double chirp experiment where a precise dual-pulse generator was employed to initiate two modulation voltage ramps and to trigger one oscilloscope beam with the first and the other beam with the second pulse. The dual-trace oscilloscope display shows the first and second demodulated chirps, as illustrated in Fig. 14. The important observation here is the similarity of these signals; in fact, no deviation between traces A and B is noticeable except for a uniform delay in the time scales. (This delay is due to the fact that trace A is triggered on the front slope of the first clock pulse, while trace B is triggered on the back slope of the second clock pulse).

The delay between the chirps was 42 μs throughout the experiment. The random variations of the relative optical phase between master and reference laser are not noticeable; i.e., the parasitic FM modulation has insignificant contributions above 25 kHz. This indicates that the mechanical vibration of the resonator structure which is the major cause of the short-term FM noise is confined to frequencies well below 25 kHz which is not surprising in view of the rigid resonator construction of both lasers. It was, in fact, observed that the FM noise of our lasers was mainly due to fluctuations in the discharge current brought on by power supply ripple which yielded frequency excursions of ± 150 kHz at a 120 Hz rate, twice the line frequency. Figure 15 illustrates this observation, showing the noise spectrum with and without line synchronization of the spectrum analyzer sweep.

3.4 Summary

While the overall task of providing a highly linear and optically coherent train of repetitively chirped pulses requires a considerable amount of additional work, the results of this six-month investigation are very encouraging for the future progress of that program. It has been established that the proposed phase sampling method is in principle adequate to implement frequency locking between the chirped master oscillator and a stable reference laser and thus ensure relative optical coherence. The continuing improvement and redevelopment of the UARL waveguide lasers has led to a frequency-chirped, sealed-off, reliable laboratory device of relatively long life and 300 mW output power. For the continuation of this program towards the fabrication of a deliverable master oscillator unit, it is recommended to first build a compact resonator in order to obtain a wide chirp band and then implement phase and ramp control loops for a wave format of the required quality.

FIG. 14

DOUBLE CHIRPS

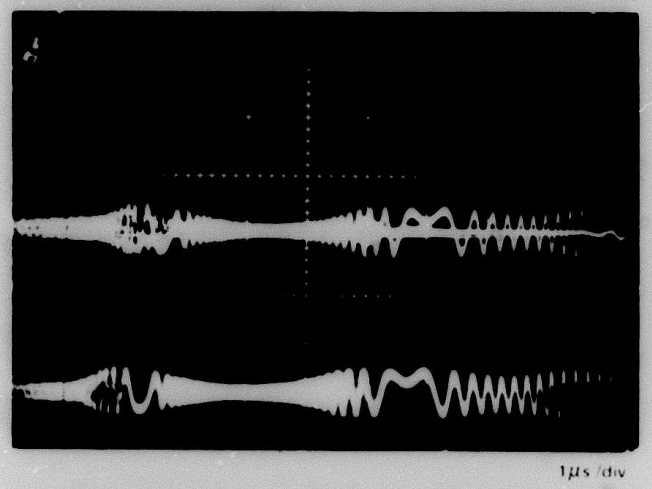

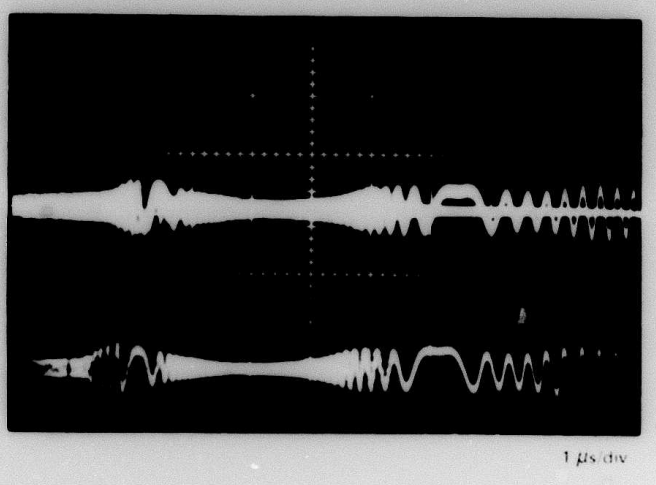

TRACE A SYNCHRONIZED WITH 1ST VOLTAGE RAMP

TRACE B, SYCHRONIZED WITH 2ND VOLTAGE RAMP 42 μs LATER

N09-122-1

FIG. 15

FM NOISE SPECTRUM

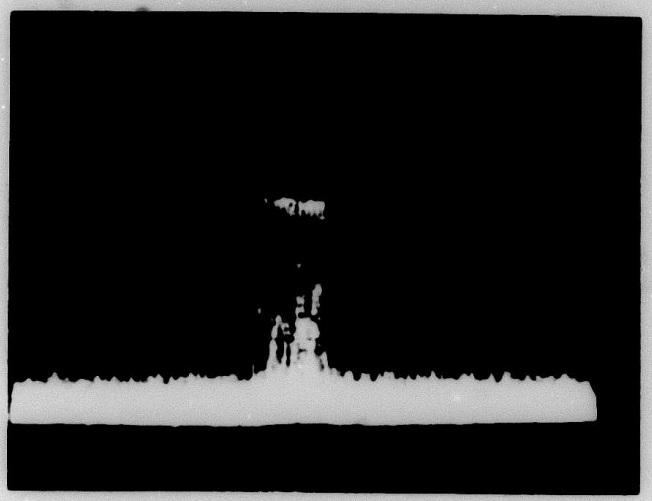

300 kHz/div

a) SPECTRAL ANALYSER SWEEP ON INTERNAL SYNC.

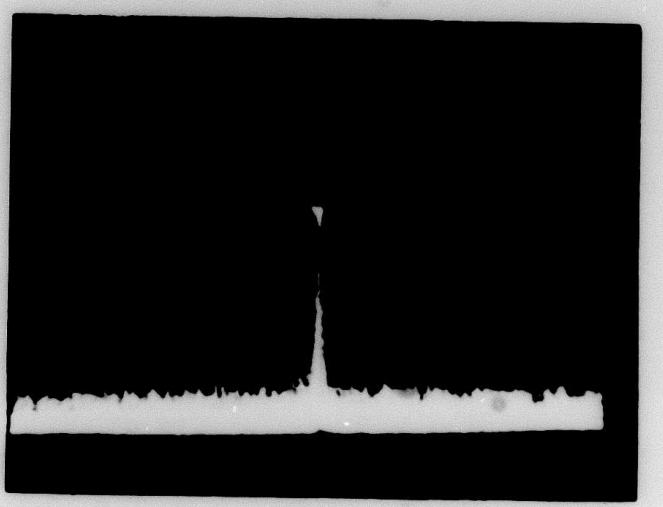

300 kHz/div

b) SPECTRAL ANALYSER SWEEP ON LINE SYNC.

N09–140–1

4.0 REFERENCES

1. Gilmartin, T. J., MIT Lincoln Laboratory, private communication.

2. Freed, C.: Design and Experiments Relating to Stable Gas Lasers, Proc. of Frequency Standards and Metrology Seminar, Univ. Laval, Quebec, Canada (30 August 1972).

3. Siegman, A.E.: Introduction to Masers and Lasers, McGraw-Hill (1971).

4. Smith, P. W.: A Waveguide Gas Laser, Appl. Phys. Lett., 19, 132 (Sept. 1972).

5. Burkhardt, E. G., T. J. Bridges, and P. W. Smith : BeO Capillary CO_2 Waveguide Laser, Optics Communications, 6, pp. 193-195 (1972).

6. Abrams, R. L. and W. B. Bridges : Characteristic of Sealed-Off Waveguide CO_2 Lasers, IEEE Journal of Quantum Electronics, QE-9, 940-946 (1973).

7. Kaminow, I. P. and E. H. Turner: Electro-Optic Light Modulators, Proc. IEEE 54, (October 1966).

8. II-VI, Inc., private communication.

9. Abrams, R. L.: Coupling Losses in Hollow Waveguide Laser Resonators, IEEE J. Quant. Electron. QE-8, 838 (Nov. 1972).

10. Smith, P. W., P. J. Maloney and O. R. Wood II: Waveguide TEA Lasers, Applied Physics Letters 23, 524-526 (Nov. 1973).

APPENDIX I

THERMAL DRIFT

Heating of the modulator crystal causes a change in its optical length; i.e., a change in the oscillating frequency if the modulator is mounted inside the optical resonator. The heating mechanisms of importance are; ohmic losses of the applied field and optical absorption inside the crystal. Since the crystal considered here is 4 cm long; the absorption coefficients is 0.2 percent/cm and the unidirectional intracavity power approximately 10 W, the total absorbed power is 0.16 W. To calculate the electrical loss we must obtain an effective resistance for the sawtooth signal. The dc resistance of our laboratory modulator is $9 \times 10^7 \Omega$. The sawtooth signal is equivalent to a spectral continuum which peaks at $f = 1/T_R$ and falls off to approximately 10 percent of peak value at $f = 3 \times 1/T_R$, where T_R is the sawtooth period.

For the referenced radar wave, $1/T_R = 300$ kHz; hence, spectral components up to 1 MHz must be taken into consideration. We, therefore, use an effective resistance value estimated at $R_{eff} = 10^7 \Omega$. The electrical power loss then is given by

$$P_{EL} = \frac{1}{T_R} \int_0^{T_R} \frac{1}{R_{eff}} \left(\frac{V_{max}}{T_R} \right)^2 dt = \frac{1}{3} \frac{V_{max}^2}{R_{eff}} \qquad \text{(I-1)}$$

Inserting the values $V_{max} = 4.5\ 10^3$ V (Section 3.2) and $R_{eff} = 10^7 \Omega$, we calculate $P_{EL} = 0.7$ W. Note that the ohmic loss is significantly larger than the optical loss.

To hold the modulator crystal at a low temperature, efficient cooling must be employed. Our laboratory modulator is placed between copper plates at the electrode faces and BeO walls at the other two side faces. The thermal conduction into these elements is of the order of 0.1 W per cm^2 of surface area and ^oC of temperature difference across the contact; the heat transport across the total surface area of our crystal is $K = 0.5$ W/^oC. Assuming that the holding structure has a large thermal mass, the crystal temperature falls off exponentially from its initial value, as

$$\theta = \theta_o \, e^{-t/\tau} \, , \qquad \text{(I-2)}$$

where τ is given by the ratio of the thermal mass of the crystal to the heat transport parameter K. From the weight of our crystal, 2.9 gram, and the specific heat of CdTe, 0.16 Wsec/g °C, we get for the thermal mass m_θ = 0.5 Wsec/°C; and for the characteristic cooling time then τ = 1 sec. Since the characteristic cooling time is orders of magnitude longer than the ramp period, equilibrium holds only for an average temperature while the instantaneous crystal temperature is determined by the instantaneous drive power.

During one chirp the crystal temperature varies as

$$\Delta\theta = \frac{1}{3} \, \frac{V_{max}}{m_\theta \cdot R_{eff} \cdot T_R^2} \cdot t^3 \, . \qquad \text{(I-3)}$$

Inserting m_θ = 0.5 Wsec/°C; V_{max} = 4.5 10^3V; T_R = 3.3 10^{-6} sec, we obtain

$$\Delta\theta = 1.25 \times 10^{11} \cdot t^3 \, . \qquad \text{(I-4)}$$

At the end of the ramp period, $t=T_R$, the temperature difference attains its maximum value of $\Delta\theta_{max}$ = 4.5 10^{-0} °C. The concomitant relative change in the optical frequency is

$$\Delta f/_f = (dn/_{d\theta} + \alpha n) \ell \cdot \Delta\theta/_L \, , \qquad \text{(I-5)}$$

where n is the index of refraction of CdTe, dn/dθ its thermal coefficient, L the optical length of the resonator, α the linear coefficient of expansion and ℓ the length of the crystal. Substituting the values f = 3 10^{13} Hz, dn/dθ = 4 x 10^{-5}/°C, α = 5 x 10^{-6}/°C, n = 2.62, ℓ = 4.0 cm and L = 30 cm, we get

$$\Delta f = 2 \times 10^8 \, \Delta\theta \, . \qquad \text{(I-6)}$$

The maximum thermal frequency excursion occurring at the end of the ramp period is then

$$\Delta f_{max} = 900 \text{ Hz} . \qquad \text{(I-7)}$$